Photoassociation of ^{85}Rb atoms into 0_u^+ states near the 5S+5P atomic limits

Photoassociation of ^{85}Rb atoms into 0_u^+ states near the 5S+5P atomic limits

T Bergeman[1]**, J Qi**[2,4]**, D Wang**[2]**, Y Huang**[2]**, H K Pechkis**[2]**, E E Eyler**[2]**,
P L Gould**[2]**, W C Stwalley**[2]**, R A Cline**[3,5]**, J D Miller**[3,6]** and D J Heinzen**[3]

[1] Department of Physics and Astronomy, SUNY, Stony Brook, NY 11794-3800, USA
[2] Department of Physics, University of Connecticut, Storrs, CT 06269-3046, USA
[3] Department of Physics, University of Texas, Austin, Texas 78712, USA

Abstract
New photoassociation data on the 0_u^+ levels of Rb_2 below the 5S+5P$_{1/2}$ limit
are combined with older data (Cline *et al* 1994 *Phys. Rev. Lett.* **73** 632) in a fit
to potentials and spin–orbit functions. The P$_{1/2}$ data exhibit oscillations in the
$B(v)$ values due to coupling between the two 0_u^+ series, as modelled accurately
by a coupled potentials approach. The fitted value for the C_3 dispersion
parameter from the combined data agrees well with the value derived from the
pure long-range 0_g^- state.

S This article has associated online supplementary data files

1. Introduction

The availability of laser-cooled atoms has made it possible to obtain high-resolution spectra
from photoassociation (PA) of atoms into molecular bound states near the dissociation limit.
Such data provide information on the long-range excited state molecular potentials and are
useful in designing methods for producing cold molecules by photoassociation processes
(Nikolov *et al* 1999, Nikolov *et al* 2000, Comparat *et al* 2000, Laburthe Tolra *et al* 2001,
Wang *et al* 2004, Sage *et al* 2005). Data from photoassociation experiments locate excited
state levels and also can lead to approximate potentials from which Franck–Condon factors
can be calculated.

　　The information obtainable from PA experiments varies with the circumstances (see, for
example, the review articles by Stwalley and Wang (1999) and Jones *et al* (2006)). For
homonuclear alkali dimers, there has been interest in the pure long-range states (Stwalley *et al*
1978), whose inner turning point is beyond the Le Roy radius inside which the atomic
wavefunctions begin to overlap. Cold atom PA techniques have provided data on the bound

vibrational levels of the 1_u states associated with the $P_{3/2}$ limit of K_2 (Wang *et al* 1998) and Cs_2 (Comparat *et al* 2000), and for 0_g^- states associated with the $P_{3/2}$ limit of Na_2 (Ratliff *et al* 1994), K_2 (Wang *et al* 1997), Rb_2 (Cline *et al* 1994, Fioretti *et al* 2001, Gutterres *et al* 2002) and Cs_2 (Fioretti *et al* 1999, Pichler *et al* 2004), yielding reliable potential curves for these states. For more deeply bound states, it has been possible to determine the dispersion parameters for the long-range part of the potential, typically using the Le Roy–Bernstein (Le Roy and Bernstein 1970) asymptotic expansion. This has been done for the $P_{3/2}1_g$ states of K_2 (Pichler *et al* 2003), Rb_2 (Cline *et al* 1994, Amiot 1995) and Cs_2 (Comparat *et al* 1999, Pichler *et al* 2004b), for the $P_{3/2} 0_u^+$ state of Cs_2 (Comparat *et al* 1999, Pichler *et al* 2004b), for the Na_2 $P_{1/2} 0_u^+$ state (Tiemann *et al* 1996), the Rb_2 $P_{1/2} 0_g^-$ (Jelassi *et al* 2006a) and 0_u^+ (Jelassi *et al* 2006b) states, as well as for the 0_g^- (Drag *et al* 2000, Pichler *et al* 2004a), 0_u^+ (Pichler *et al* 2004a) and 1_g (Pichle r*et al* 2004a) states of Cs_2 below the $6P_{1/2}$ limit.

In this study, we present new experimental data on the photoassociation of ^{85}Rb atoms to 0_u^+ resonances below the $5S+5P_{1/2}$ limit and present an analysis of the new data together with previously reported data (Cline *et al* 1994) on PA of Rb atoms below the $5S+5P_{3/2}$ limits. The two 0_u^+ states are coupled by a spin–orbit function and can interestingly be considered together. In contrast with the elegant asymptotic quantum defect analysis of Jelassi *et al* (2006b), the data presented here raise new issues and challenges for two reasons: (1) the data extend far enough below the Rb $5S+5P_{1/2}$ limit that the asymptotic expansion becomes invalid and a coupled potentials model is required; (2) including also the earlier data from below the Rb $5S+5P_{3/2}$ limit in the model raises questions of consistency in the optimization process, but does provide a reconciliation between the earlier value (Cline *et al* 1994) for the C_3 coefficient for the Rb($5S+5P$) atomic limit and the value obtained more recently from the pure long-range 0_g^- state (Gutterres *et al* 2002).

2. Experimental procedure and data

The experimental ^{85}Rb$_2$ photoassociation (PA) spectra from Storrs are obtained using trap loss in two distinct diode-laser-based magneto-optical traps (MOTs) which are continuously loaded from background Rb vapour (Huang *et al* 2006, Lozeille *et al* 2006, Wang *et al* 2004a). The loading times for the MOTs range from 3 to 5 s. The trapped samples, at densities and temperatures of 10^{10} to 10^{11} cm^{-3} and <200 μK, respectively, are illuminated with $\approx$500 mW of light from a tunable single-frequency Ti-sapphire laser. When this light is tuned to a PA resonance, pairs of free atoms are promoted to an excited molecular state and subsequently decay, either back into free atoms with increased kinetic energy or into a bound molecule. In either case, the loss of atoms from the trap results in a dip in the MOT fluorescence.

Some regions of the trap-loss spectrum have been measured using a normal MOT, while others have utilized a dark SPOT (SPontaneous force Optical Trap) (Ketterle *et al* 1993) which generally yields higher densities. The PA spectra from the dark SPOT are shifted relative to the spectra from the normal MOT by the 3.036 GHz ^{85}Rb ground-state hyperfine splitting, since the atoms in the dark region reside predominantly in the lower ($F = 2$) hyperfine level. The absolute frequencies of the PA resonances are calibrated to within 0.02 cm^{-1} using I_2 spectroscopy.

The data scans include transitions to 0_g^- and 1_g as well as to 0_u^+ PA resonances. Here we focus on just the 0_u^+ series. Rotationally resolved data from 60 0_u^+ bands below the $5S+5P_{1/2}$ limit were obtained. Examples are shown in figure 1. Note that the relative intensity of the rotational lines varies, especially near the dissociation limit. Values for the band origins, $G(v)$, and rotational parameters, $B(v)$, are given in table 2.
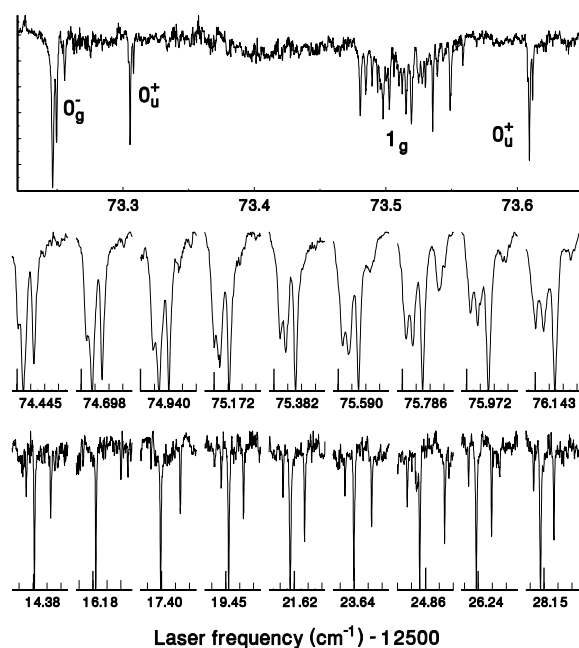
Figure 1. Experimental data below the 5S+5P$_{1/2}$ limit, which is nominally at 12 579.00 cm^{-1} (Barwood *et al* 1991). Top: part of a scan showing the different forms of 0_g^-, 0_u^+, and 1_g bands (only the 1_g bands have an appreciable hyperfine structure). Middle: 0_u^+ bands near the dissociation limit. Bottom: 0_u^+ bands at lower energies. The numbers indicate the laser energy (less 12 500 cm^{-1}, as indicated) for the thickest tick mark in each scan. The other tick marks represent intervals of 0.003 (0.01) cm^{-1} for the upper (lower) set.

The Rb$_2$ 0_u^+ data below 5S+5P$_{3/2}$ were obtained at the University of Texas, as previously reported (Cline *et al* 1994). The Texas data were obtained with a far-off resonance trap (FORT) employing one fixed frequency laser, plus a second laser with 1 MHz bandwidth, to scan over the PA resonances. The two lasers were modulated alternately at 200 kHz to eliminate power broadening and shifts. Resonances were detected by reductions in the atomic fluorescence (trap loss). These resonances are broadened by pre-dissociation, and thus are more extensively overlapped than the PA resonances below 5P$_{1/2}$. PA signals for 0_u^+ resonances that are not strongly overlapped with 0_g^- and 1_g resonances are shown in figure 2. Table 3 lists the 0_u^+ resonance line positions together with residuals from a fit from a coupled potentials model discussed below.

3. Analysis of the data

To provide a perspective on the regime of energy and internuclear distance relevant here, we give in figure 3 approximate potentials for the Rb$_2$ A and b states and for the region near the 5S+5P atomic limit.

3.1. Results from fits to Le Roy–Bernstein expressions

In analysing the data, we consider as a first approximation the Le Roy–Bernstein semiclassical method (Le Roy and Bernstein 1970). According to Marinescu and Dalgarno (1995), for
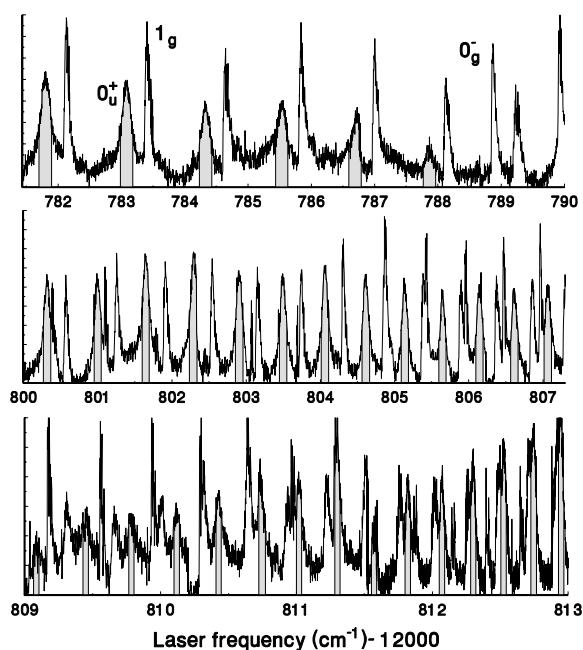
Figure 2. Experimental data scans over resonances below the 5S+5P$_{3/2}$ limit, which is nominally at 12 816.603 cm^{-1} (Barwood *et al* 1991). The 0_u^+ resonances are denoted by filled-in areas. Between 12 789 and 12 800 cm^{-1} and between 12 807 and 12 809 cm^{-1}, the 0_u^+ bands are strongly overlapped by 0_g^- bands, while beyond 12 813 cm^{-1}, the 0_u^+ bands are overlapped with 1_g bands.
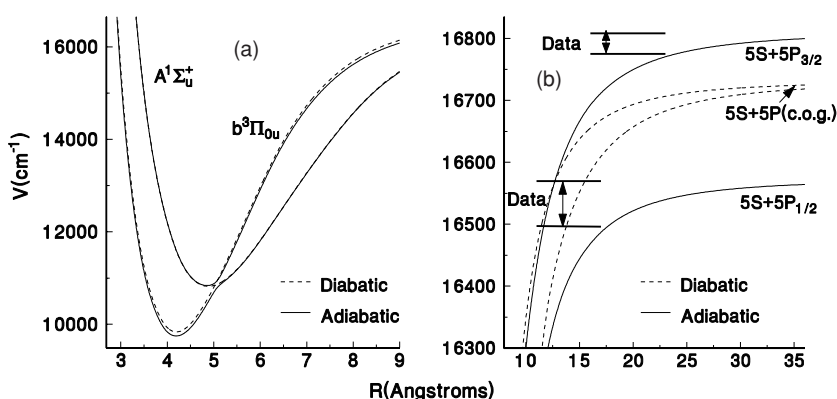

Figure 3. Potentials as obtained from the final fitted parameters and *ab initio* results of Edvardsson *et al* (2003). Energies are relative to the minimum of the X state, and thus include the X state dissociation energy of 3993.53(6) cm^{-1} (Tsai *et al* 1997). Part (a) gives an overall view of the potentials for the $A^1\Sigma_u^+$ and the $\Omega = 0$ component of the $b^3\Pi_u$ states. Part (b) shows more details of the region near the 5S+5P dissociation limit. The diabatic potentials (dashed line) are purely non-relativistic. The adiabatic potentials are obtained by diagonalizing the 2×2 matrix containing the diabatic potentials and the spin–orbit coupling function, as in (1).

alkali molecules tending to the lowest S+P atomic limit, there are two C_3 quantities differing by a factor of -2 if one neglects relativistic effects: $C_3(\sigma) = -2C_3(\pi)$. The effect of spin–orbit coupling between 0_u^+ states tending to P$_{3/2}$ and P$_{1/2}$ atomic limits has been discussed by

Marinescu and Dalgarno (1996) and by Aubert-Frécon *et al* (1998). The following is a brief summary and application to the 0_u^+ states of Rb$_2$.

For the 0_u^+ manifold, one has a 2 by 2 Hamiltonian matrix. Neglecting rotation, it is

$$H = \begin{matrix} ^1\Sigma_u^+ \\ ^3\Pi_{u0} \end{matrix} \begin{pmatrix} V\left(^1\Sigma_u^+\right) & \Delta_{\Pi\Sigma} \\ \Delta_{\Pi\Sigma} & V\left(^3\Pi_{1u}\right) - \Delta_{\Pi\Pi} \end{pmatrix},$$

$$\Delta_{\Pi\Pi} \xrightarrow{R\to\infty} \frac{\Delta}{3} \qquad \Delta_{\Pi\Sigma} \xrightarrow{R\to\infty} \frac{\sqrt{2}\Delta}{3}, \tag{1}$$

where the $V\left(^1\Sigma_u^+\right)$ and $V\left(^3\Pi_u\right)$ are Born–Oppenheimer potentials (possibly including relativistic mass corrections, but not spin–orbit effects), Δ is the atomic spin–orbit splitting of the P state, and $\Delta_{\Pi\Pi}$ and $\Delta_{\Pi\Sigma}$ are functions of the internuclear separation, R, that express diagonal and off-diagonal spin–orbit effects.

Asymptotically, the (non-relativistic) potentials behave as

$$V\left(^1\Sigma_u^+\right) \to E^0 - \frac{C_3(\sigma)}{R^3}, \qquad V\left(^3\Pi_u\right) \to E^0 - \frac{C_3(\pi)}{R^3} \tag{2}$$

where E^0 is the centre-of-gravity of the P levels.

As discussed in Gutterres *et al* (2002), the C_3 parameters are related to the dipole transition moments for either P$_j$ state,

$$M_j^2 = |\langle 5s|r|5p_j\rangle|^2 = \frac{9\hbar}{4\tau_j}\left(\frac{\lambda_j}{2\pi}\right)^3 \tag{3}$$

where τ_j is the radiative lifetime and λ is the wavelength of the 5P$_j$ $\to$ 5S transition. Thus,

$$C_3(\pi) = -\frac{M_{3/2}^2}{4}, \qquad C_3(\sigma) = \frac{M_{1/2}^2}{2}. \tag{4}$$

As also discussed in Gutterres *et al* (2002), the $\langle s|r|p_j\rangle$ moments are not exactly identical because of relativistic effects in the wavefunctions. Estimates of the differences range from 2.3×10^{-4} to 2.2×10^{-3}. In this study, these effects are masked by uncertainties in the short-range potential.

Neglecting now the R-dependences of the spin–orbit functions, we substitute (2) into (1). In doing so, we assume that $|\Delta| > 2C_3/3R^3$, as is the case over a considerable range of R for the Rb$_2$ states of interest here. We obtain

$$V(\mathrm{P}_{1/2}) - E^0(^2\mathrm{P}_{1/2}) \to -\frac{C_3(\sigma) + 2C_3(\pi)}{3R^3} \approx -\frac{4C_3(\pi)}{3R^3},$$

$$V(\mathrm{P}_{3/2}) - E^0(^2\mathrm{P}_{3/2}) \to -\frac{C_3(\pi) + 2C_3(\sigma)}{3R^3} \approx -\frac{5C_3(\pi)}{3R^3}. \tag{5}$$

For the levels studied here, there are departures from these idealized expressions due to departures of the potentials from a precise C_3/R^3 form, R-dependence of the spin–orbit functions, and effects of the inner wall.

As reported in Cline *et al* (1994), the 0_u^+ states near the 5S+5P$_{3/2}$ atomic limit fit quite nicely to the semiclassical expression derived by Le Roy and Bernstein (1970),

$$v_D - v = \frac{4a_3}{h}\sqrt{2\mu}\,C_3^{1/3}[D - E(v)]^{1/6}, \qquad a_3 = \frac{\sqrt{\pi}\,\Gamma(5/6)}{2\Gamma(4/3)} = 1.120\,2513, \tag{6}$$

applied to a potential of the form $V(R) = D - C_3/R^3$. If one writes $v_D - v = K[D - E(v)]^{1/6}$, then if D and $E(v)$ are in cm^{-1} and C_3 is in atomic units, $K = 36.1269\,C_3^{1/3}$. Row 2 of table 1 gives the fitted value of C_3 from Cline *et al* (1994), multiplied by 0.6 to be consistent with (5),
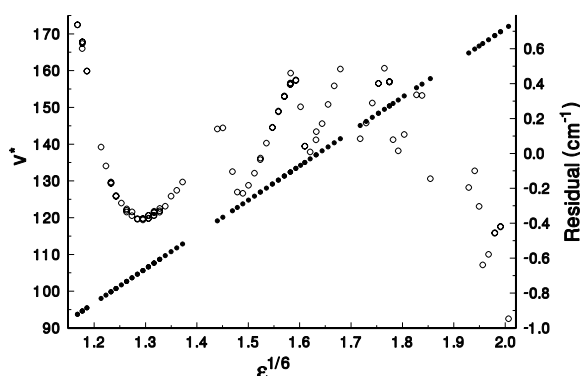
Figure 4. Results of a fit of the 0_u^+ data below the 5S+5P$_{1/2}$ limit to the semiclassical model of (6). The full circles and left axis show $v^* = v_D - v$ versus $[\epsilon = D - E(v)]^{1/6}$, while the open circles and right axis show the residuals of this fit.

Table 1. C_3 values (in au) obtained from previous studies and from the present work. All values are stated in atomic units, and apply to $C_3(\pi)$. Uncertainty limits for results from the present work are not stated because of the high degree of correlation between the various fitted parameters.

Source	$C_3(\pi)$
Theory (Marinescu and Dalgarno 1995)	9.202
Experiment (Cline *et al* 1994)	8.784(6)
Experiment (Gutterres *et al* 2002)	8.905(26)
This work: Coupled potentials fit to $P_{1/2}$ 0_u^+ data	8.948
This work: Fit to combined $P_{1/2}$ and P$_{3/2}$ data	8.903[a]

[a] Preferred result from the present work.

but excluding the 'systematic' uncertainty of 0.4 au quoted in Cline *et al* (1994). As stated in Cline *et al* (1994), one expects that even for 0_u^+ levels below 5P$_{3/2}$, other potential terms will enter, so this value differs from values obtained from results obtained from experimental data on the pure long-range 0_g^- state (Gutterres *et al* 2002), also listed in table 1.

Levels below the 5S+5P$_{1/2}$ atomic limit can also be fit to the expression given in (6), and a nearly straight-line plot of $v_D - v$ versus $[D - E(v)]^{1/6}$ results, as shown in figure 4. However, the deviations, which are plotted in this figure relative to the right axis, are large compared with the experimental uncertainty, and show systematic effects that give a nearly oscillatory behaviour.

3.2. Fitting procedure with a coupled potentials model

To understand the residuals in figure 4, we consider various approximations to the relevant potentials and spin–orbit functions. Bound state eigenvalues are calculated by the discrete variable representation (DVR) (Colbert and Miller 1992) approach, with an appropriate scaling of the R coordinate to increase the density of points where the momentum is greatest (Tiesinga *et al* 1998). For metastable (pre-dissociating) states above the 5P$_{1/2}$ limit, the use of an absorbing potential (Monnerville and Robbe 1994) used in previous work (Bergeman *et al* 2002) did not yield stable results as a function of the position of the imaginary potential terms, so we choose to calculate scattering phase shifts with a two-channel renormalized Numerov

Table 2. $G(v)$ and $B(v)$ values measured from the PA spectrum below the $5P_{1/2}$ limit. Column 1 gives an arbitrary numbering which indicates the gaps in the data. Column 2 is the laser energy in cm^{-1} for the $J = 0$ line. This number plus the ground state $D_e = 3993.53$ cm^{-1} from Tsai *et al* (1997) is taken as $G(v)$. Column 3 gives the differences between calculated and observed $G(v)$ values. Column 4 is $10^3 B(v)$ in cm^{-1}, and column 5 gives the difference, calculated less observed for $10^3 B(v)$. The calculated values are from a fit with $C_3(P_{1/2}) = 8.945$ au. Energies and $B(v)$ values are in cm^{-1}.

n	$E_{L,J=0}$	Cal-Ob	$10^3 B(v)$	Cal-Ob	n	$E_{L,J=0}$	Cal-Ob	$10^3 B(v)$	Cal-Ob
9	12 514.375	0.013	2.9310	−0.0926	51	12 564.666	0.002	1.2470	−0.0977
11	12 517.393	0.008	3.4485	0.0004	52	12 565.321	0.004	1.1980	−0.1212
12	12 519.447	0.007	2.6895	−0.0856	53	12 565.955	0.004	1.1775	−0.1456
13	12 521.612	0.001	2.5960	−0.0719	54	12 566.565	0.005	1.0750	−0.0736
14	12 523.594	−0.009	3.2035	−0.1475	55	12 567.153	0.002	0.9568	0.0261
15	12 524.807	−0.012	4.4735	−0.1710	56	12 567.711	0.004	1.0330	−0.0523
16	12 526.233	−0.005	2.7605	−0.0511	57	12 568.244	0.004	1.0600	−0.0491
17	12 528.143	−0.008	2.4440	−0.1006	58	12 568.746	0.003	1.1385	−0.0166
24	12 538.980	−0.013	2.4040	−0.1290	59	12 569.205	0.002	1.4615	−0.0168
26	12 541.082	−0.006	3.0430	−0.0325	60	12 569.600	−0.002	2.0065	−0.0715
27	12 542.408	−0.013	2.0725	−0.0069	62	12 570.346	0.002	1.2260	−0.0233
29	12 545.232	−0.011	1.8885	−0.0429	63	12 570.753	0.004	1.0045	−0.0516
30	12 546.552	−0.009	2.0705	−0.0873	69	12 572.983	0.004	0.6365	0.0037
31	12 547.649	0.005	3.0930	−0.1228	70	12 573.304	0.003	0.6305	−0.0121
32	12 548.411	0.003	3.1760	−0.0225	71	12 573.608	0.005	0.6075	−0.0087
33	12 549.443	−0.007	2.0170	−0.0442	72	12 573.906	−0.002	0.6323	−0.0510
34	12 550.619	−0.009	1.6680	0.0253	73	12 574.180	0.003	0.5555	0.0102
35	12 551.784	−0.007	1.6320	−0.0238	74	12 574.450	−0.002	0.5379	0.0145
36	12 552.911	−0.007	1.5610	0.0303	75	12 574.699	0.002	0.5490	−0.0072
37	12 553.977	−0.006	1.6785	0.0153	76	12 574.943	−0.001	0.6355	−0.1010
41	12 557.249	−0.002	1.5155	0.0082	77	12 575.172	−0.002	0.5270	0.0049
42	12 558.174	−0.002	1.3030	0.0890	78	12 575.383	0.004	0.5780	−0.0422
43	12 559.075	−0.001	1.2970	0.0360	79	12 575.595	−0.001	0.5722	−0.0227
44	12 559.946	−0.003	1.2870	0.0210	80	12 575.787	0.001	0.6795	−0.1017
45	12 560.774	0.001	1.3615	−0.0343	81	12 575.974	−0.002	0.6228	0.0046
46	12 561.555	0.000	1.6284	−0.1549	82	12 576.145	−0.002	0.8575	−0.1537
47	12 562.239	0.003	2.0889	−0.0088	83	12 576.308	−0.004	0.8016	−0.0029
48	12 562.770	0.004	2.7780	−0.1733	84	12 576.462	−0.009	0.8648	0.0043
49	12 563.336	0.002	1.8245	−0.0816	87	12 576.872	−0.008	0.7010	−0.0569
50	12 563.995	0.002	1.4010	−0.1009	88	12 576.995	−0.002	0.5773	−0.0339

method (Johnson 1973, 1978, 1985). Resonance positions are indicated by maxima of the energy derivative of these phase shifts. By comparing the eigenvalues and resonance energies with the observations, the potentials and spin–orbit functions can be adjusted to optimally fit the experimental data.

The available PA data lie within 70 cm^{-1} of the $5P_{1/2}$ limit, and within 30 cm^{-1} of the $5P_{3/2}$ limit, while the relevant potentials, for the $A^1\Sigma_u^+$ and $b^3\Pi_{0u}$ state, are calculated to be 5800 and 6800 cm^{-1} deep, respectively. In contrast to lighter alkali dimer molecules (Na$_2$ and K$_2$), these Rb$_2$ states have not been well characterized by analysis of spectroscopic data from absorption of ground-state molecules. Clearly, the present data cannot determine the deeper parts of the potentials, so our interpretation of the 0_u^+ PA resonances necessarily makes use of *ab initio* potentials. We employ those calculated by Lunell and colleagues (Edvardsson *et al* 2003).

Table 3. 0_u^+ band energy levels measured from the PA spectrum below the $5P_{3/2}$ limit. Columns 1 and 4 give the measured laser energy, columns 2 and 5 the residuals from the fit to the coupled potentials model, and columns 3 and 6 the estimated experimental uncertainty. Many highly blended bands are excluded in this listing. All quantities are in cm^{-1}.

E_L	Residual	σ	E_L	Residual	σ
12 781.8041	0.1061	0.0038	12 811.0190	−0.0293	0.0150
12 783.0791	0.0828	0.0033	12 811.3010	−0.0264	0.0240
12 784.3310	0.0774	0.0046	12 811.5720	−0.0229	0.0600
12 785.5326	0.0616	0.0060	12 811.8190	−0.0320	0.0360
12 786.6923	0.0426	0.0096	12 812.0710	−0.0254	0.0360
12 800.3165	−0.0031	0.0031	12 812.3010	−0.0302	0.0360
12 800.9989	−0.0046	0.0032	12 812.5240	−0.0317	0.0150
12 801.6480	−0.0153	0.0022	12 812.7460	−0.0246	0.0240
12 802.2872	−0.0124	0.0043	12 812.9480	−0.0279	0.0270
12 802.9057	−0.0133	0.0038	12 813.1420	−0.0302	0.0270
12 803.4959	−0.0142	0.0025	12 813.3340	−0.0256	0.0360
12 804.0644	−0.0154	0.0026	12 813.5210	−0.0176	0.0360
12 804.6126	−0.0162	0.0025	12 813.6840	−0.0254	0.0360
12 805.1371	−0.0206	0.0020	12 813.8540	−0.0184	0.0360
12 805.6464	−0.0177	0.0025	12 813.9990	−0.0288	0.0360
12 806.1442	−0.0107	0.0042	12 814.1480	−0.0279	0.0240
12 806.6129	−0.0144	0.0027	12 814.2910	−0.0260	0.0180
12 807.0645	−0.0174	0.0032	12 814.4295	−0.0220	0.0150
12 809.0848	−0.0210	0.0031	12 814.5620	−0.0174	0.0180
12 809.4485	−0.0159	0.0038	12 815.9152	−0.0141	0.0090
12 809.7842	−0.0243	0.0027	12 815.9630	−0.0171	0.0090
12 810.1176	−0.0192	0.0023	12 816.0015	−0.0264	0.0090
12 810.4260	−0.0273	0.0150	12 816.0430	−0.0299	0.0090
12 810.7310	−0.0261	0.0150			

Since the *ab initio* potential functions are not determined to spectroscopic accuracy, adjustments are justified. For example, the potential energy minima are undoubtedly uncertain to ≈ 50 cm^{-1} and can thus be adjusted over this range. An adjustable extrapolation for the inner walls was also used. For the long-range part, the C_n parameters have been determined quite accurately, but small adjustments can be made consistent with the stated uncertainty limits. The exchange parameters, which are not accurately determined in previous studies, have also been adjusted to fit the data.

After various attempts to employ spin–orbit functions of Morse potential form, we eventually used *ab initio* results obtained for analogous states of K$_2$ (Manaa *et al* 2002), scaled to give the known Rb 5^2P fine structure splitting. The variation of these functions about the known asymptotic (atomic) limit was adjusted in the fitting process, and the sharp change at the last calculated value was smoothed somewhat. The resulting functions are shown in figure 5.

The effect of the coupling between the 0_u^+ states dissociating to 5S+5P$_{1/2}$ and to 5S+5P$_{3/2}$ is shown most dramatically in a plot of $B(v)$ values, given in figure 6. The solid line and small circles denote values obtained from a fit to only the data below the 5P$_{1/2}$ limit. In this plot, the larger $B(v)$ values are associated with states that have the most P$_{3/2}$ character, which are most tightly bound in this energy region. Points for which data are missing are those for which the PA excitation amplitude is very small due to small overlap of the initial and PA resonance
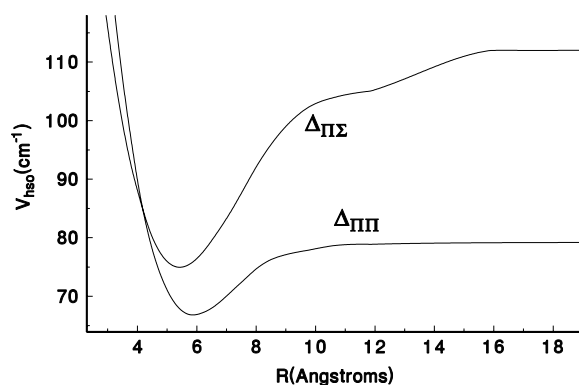
Figure 5. The diagonal ($\Delta_{\Pi\Pi}$) and off-diagonal ($\Delta_{\Sigma\Pi}$) spin–orbit functions used in this work. They are the functions obtained (by scaling adjustments of *ab initio* calculations) in the study of K$_2$ A and b states (Manaa *et al* 2002), scaled so that the asymptotic limits match the values expected from the Rb 5P atomic fine structure splitting.
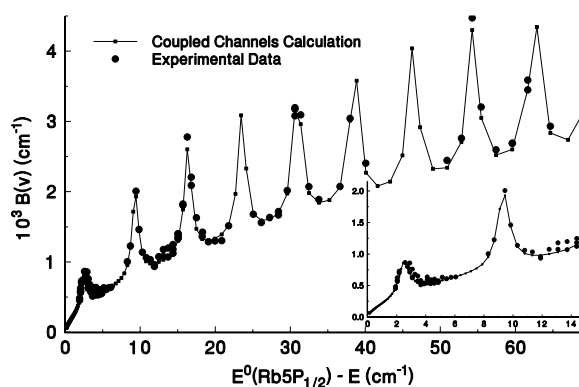

Figure 6. Experimental (larger solid circles) $B(v)$ values as compared with results of a coupled channels calculation (dots and solid line) using fitted potential parameters and the spin–orbit functions shown in figure 5.

wavefunctions. Very similar plots of Rb$_2$ 0_u^+ $B(v)$ values have been obtained by Kokoouline *et al* (1999, 2000) from purely theoretical calculations.

Efforts to fit the combined 0_u^+ data sets from below the P$_{3/2}$ limit together with the data below the P$_{1/2}$ limit were not totally satisfactory. Because the rotational structure of the pre-dissociated bands was not resolved, the peak was estimated to correspond with the transition to the $J = 2$ line. Optimum adjustments of the *ab initio* potentials and spin–orbit functions differed for the two data sets, so the overall best results were a compromise, in which the residuals of each showed deviations larger than experimental uncertainties. For example, the residuals for the P$_{3/2}$ data shown in figure 7(a) show significant deviations between calculated and observed resonance energies for the lowest energies, while for these same adjusted parameters and spin–orbit functions, the residuals for the P$_{1/2}$ data were larger than when these data were fit alone (figure 7(b)). We should also mention that the best fits to the data in either region were obtained by making small shifts of the energy scales ($\approx$0.03 cm^{-1}) that undoubtedly compensate for deficiencies of the model potentials and spin–orbit functions. The residuals plotted in figure 7 and listed in tables 2 and 3 do include these shifts. Despite these less than desirable features in our analysis, the optimum value of $C_3(\pi)$
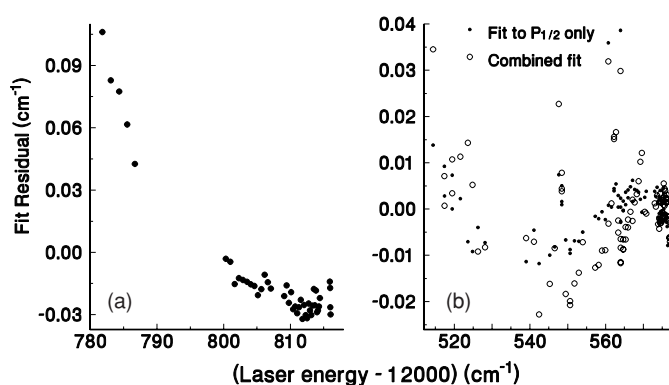
Figure 7. (a) Residuals from fits to the 0_u^+ $P_{3/2}$ data using the coupled potentials model. Experimental uncertainties are given in table 3. (b) Residuals from fits to the 0_u^+ $P_{1/2}$ data with only the $P_{1/2}$ data included (full circles) and with the combined data (open circles). Including the $P_{3/2}$ data in the fit enlarges the residuals somewhat. The rms scatter of the residuals from the fit to the $P_{1/2}$ data alone was approximately 0.006 cm^{-1}.

from such combined fits was indeed found to be restricted well within the uncertainty limits of the value obtained from the pure long-range 0_g^- state (Gutterres *et al* 2002). Our recommended value also agrees well with the value from lifetime measurements noted in this reference.

Thus a primary result of the fit to the combined data is to reduce the 'systematic uncertainty' of 0.3 au in $C_3(\pi)$ quoted in Cline *et al* (1994). The model used here includes many of the additional effects, such as the effect of the short-range potential, that were not included in the asymptotic energy model used by Cline *et al* (1994). Hyperfine structure effects, discussed with more recent data below the $5P_{3/2}$ limit of ^{87}Rb (Kemmann *et al* 2004), are not included in our model, however, and may explain some of the deviations with observations. Furthermore, there remains an undetermined amount of correlation between the $C_3(\pi)$ value obtained here and other adjustable parameters, so that meaningful uncertainty limits on this parameter cannot be given.

The fitted potentials and spin–orbit functions are given in an associated online data file (available from stacks.iop.org/JPhysB/39/S813), for use in calculating Franck–Condon factors and other properties.

In summary, we have presented new data on the photoassociation of ^{85}Rb atoms into 0_u^+ states below the $5S+5P_{1/2}$ limit, and have modelled these data together with previous data on 0_u^+ levels obtained below the $5S+5P_{3/2}$ limit, by the use of two potentials coupled by a spin–orbit function. This model confirms in detail that the 0_u^+ series tending to these two limits are coupled in such a way as to produce maxima in the rotational parameters ($B(v)$) below the $P_{1/2}$ limit where the intermixing with states tending to the $P_{3/2}$ limit is maximal. It is hoped that current work to obtain improved *ab initio* potentials and spin–orbit functions, and also to obtain and analyse spectroscopic data for lower 0_u^+ levels, will reduce the small but persistent deviations between model calculations as presented here, and experiment.

Acknowledgments

References

Amiot C 1995 *Chem. Phys. Lett.* **241** 133

Aubert-Frécon M, Hadinger G, Magnier S and Rousseau S 1998 *J. Mol. Spectrosc.* **188** 182

Barwood G P, Gill P and Rowley W R C 1991 *Appl. Phys.* B **53** 142

Bergeman T, Julienne P S, Williams C J, Tiesinga E, Manaa M R, Wang H, Gould P L and Stwalley W C 2002 *J. Chem. Phys.* **117** 7491

Cline R A, Miller J D and Heinzen D J 1994 *Phys. Rev. Lett.* **73** 632

Colbert D and Miller W 1992 *J. Chem. Phys.* **96** 1982

Comparat D, Drag C, Fioretti A, Dulieu O and Pillet P 1999 *J. Mol. Spectrosc.* **195** 229

Comparat D, Drag C, Laburthe Tolra B, Fioretti A, Pillet P, Crubeillier A, Dulieu O and Masnou-Seeuws F 2000 *Eur. Phys. J.* D **11** 59

Drag C, Laburthe Tolra B, Dulieu O, Comparat D, Vatasescu M, Boussen S, Guibal S, Crubellier A and Pillet P 2000 *IEEE J. Quantum Electron.* **36** 1378

Edvardsson D, Lunell S and Marian C M 2003 *Mol. Phys.* **101** 2381

Fioretti A, Amiot C, Dion D M, Dulieu O, Mazzoni M, Smirne G and Gabbanini C 2001 *Eur. Phys. J.* D **15** 189

Fioretti A, Comparat D, Drag C, Amiot C, Dulieu O, Masnou-Seeuws F and Pillet P 1999 *Eur. Phys. J.* D **5** 389

Gutterres R F, Amiot C, Fioretti A, Gabbanini C, Mazzoni M and Dulieu O 2002 *Phys. Rev.* A **66** 024502

Huang Y, Qi J, Pechkis H K, Wang D, Eyler E E, Gould P L and Stwalley W C 2006 *J. Phys. B: At. Mol. Opt. Phys.* **39** S857

Jelassi H, Viaris de Lesegno B and Pruvost L 2006a *Phys. Rev.* A **73** 032501

Jelassi H, Viaris de Lesegno B and Pruvost L 2006b *Phys. Rev.* A at press

Johnson B R 1973 *J. Comput. Phys.* **13** 445

Johnson B R 1978 *J. Chem. Phys.* **69** 4678

Johnson B R 1985 *Phys. Rev.* **32** 1241

Jones K M, Tiesinga E, Lett P D and Julienne P S 2006 *Rev. Mod. Phys.* at press

Kemmann M, Mistrik I, Nussmann S, Helm H, Williams C J and Julienne P S 2004 *Phys. Rev.* A **69** 022715

Ketterle W, Davis K, Joffe M, Martin A and Pritchard D E 1993 *Phys. Rev. Lett.* **70** 2253

Kokoouline V, Dulieu O, Kosloff R and Masnou-Seeuws F 1999 *J. Chem. Phys.* **110** 9865

Kokoouline V, Dulieu O, Kosloff R and Masnou-Seeuws F 2000 *Phys. Rev.* A **62** 032716

Laburthe Tolra B, Drag C and Pillet P 2001 *Phys. Rev.* A **64** 061401

Le Roy R J and Bernstein R B 1970 *J. Chem. Phys.* **52** 3869

Lozeille J, Fioretti A, Gabbanini C, Huang Y, Pechkis H K, Wang D, Gould P L, Eyler E E, Stwalley W C, Aymar M and Dulieu O 2006 *Eur. Phys. J.* D **39** 261

Lu K T and Fano U 1970 *Phys. Rev.* A **2** 81

Manaa M R, Ross A J, Martin F, Crozet P, Lyyra A M, Li L, Amiot C and Bergeman T 2002 *J. Chem. Phys.* **117** 11208

Marinescu M and Dalgarno A 1995 *Phys. Rev.* A **52** 311

Marinescu M and Dalgarno A 1996 *Z. Phys.* D **36** 239

Monnerville M and Robbe J M 1994 *J. Chem. Phys.* **101** 7680

Nikolov A N, Ensher J R, Eyler E E, Wang H, Stwalley W C and Gould P L 2000 *Phys. Rev. Lett.* **84** 246

Nikolov A N, Eyler E E, Wang X T, Li J, Wang H, Stwalley W C and Gould P L 1999 *Phys. Rev. Lett.* **82** 703

Ostrovsky V N, Kokoouline V, Luc-Koenig E and Masnou-Seeuws F 2001 *J. Phys. B: At. Mol. Opt. Phys.* **34** L27

Pichler M, Chen H M, Wang H, Stwalley W C, Ross A J, Martin F, Aubert-Frécon M and Russier-Antoine I 2003 *J. Chem. Phys.* **118** 7837

Pichler M, Chen H and Stwalley W C 2004a *J. Chem. Phys.* **121** 1796

Pichler M, Chen H and Stwalley W C 2004b *J. Chem. Phys.* **121** 6779

Pruvost L 2006 Private communication

Ratliff L P, Wagshul M E, Lett P D, Rolston S L and Phillips W D 1994 *J. Chem. Phys.* **101** 2638

Sage J M, Sainis S, Bergeman T and DeMille D 2005 *Phys. Rev. Lett.* **94** 203001

Stwalley W C, Uang Y-H and Pichler G 1978 *Phys. Rev. Lett.* **41** 1164

Stwalley W C and Wang H 1999 *J. Mol. Spectrosc.* **195** 194

Tiemann E, Knöckel H and Richling H 1996 *Z. Phys.* D **37** 323

Tiesinga E, Williams C J and Julienne P S 1998 *Phys. Rev.* A **57** 4257

Tsai C C, Freeland R S, Vogels J M, Boesten H M J M, Verhaar B J and Heinzen D J 1997 *Phys. Rev. Lett.* **79** 1245

Wang D *et al* 2004a *Eur. Phys. J.* D **31** 165

Wang D, Qi J, Stone M F, Nikolayeva O, Wang H, Hattaway B, Gensemer S D, Gould P L, Eyler E E and Stwalley W C 2004b *Phys. Rev. Lett.* **93** 243005

Wang H, Gould P L and Stwalley W C 1997 *J. Chem. Phys.* **106** 7899

Wang X, Wang H, Gould P L, Stwalley W C, Tiesinga E and Julienne P 1998 *Phys. Rev.* A **57** 4600